Applied Radiation and Isotopes 135 (2018) 61–66

Contents lists available at ScienceDirect

Applied Radiation and Isotopes

journal homepage: www.elsevier.com/locate/apradiso

# Simulation and experimental measurement of radon activity using a multichannel silicon-based radiation detector

F.B. Ozdemir[a], A.B. Selcuk[b], S. Ozkorucuklu[c], A.B. Alpat[d], T. Ozdemir[e,*], N. Özek[f]

[a] Beykent University, Istanbul, Turkey
[b] İzmir Demokrasi University, İzmir, Turkey
[c] Istanbul University, Istanbul, Turkey
[d] Sabanci University, Turkey
[e] Bartin University, Bartin, Turkey
[f] Süleyman Demirel University, Isparta, Turkey

## HIGHLIGHTS

- A new -generation semiconductor micro-strip detector was used for detecting radon (Rn-222) activity.
- Count-ADC channel, eta-charge, and dose–response graphs were experimentally obtained.
- The radon simulation in radiation detector was theoretically performed using the Geant4 software package.
- Radioactive decay, energy generation, energy values, and efficiency values were plotted using the root program.

## ARTICLE INFO

*Keywords:*
Rn-222
Radiation
Semiconductor
Silicon detector
Geant4
Root

## ABSTRACT

In this study, high-precision radiation detector (HIPRAD), a new-generation semiconductor microstrip detector, was used for detecting radon (Rn-222) activity. The aim of this study was to detect radon (Rn-222) activity experimentally by measuring the energy of particles in this detector. Count-ADC channel, eta-charge, and dose–response values were experimentally obtained using HIPRAD. The radon simulation in the radiation detector was theoretically performed using the Geant4 software package. The obtained radioactive decay, energy generation, energy values, and efficiency values of the simulation were plotted using the root program. The new-generation radiation detector proved to have 95% reliability according to the obtained dose–response graphs. The experimental and simulation results were found to be compatible with each other and with the radon decays and literature studies.

## 1. Introduction

Ionization-based detection of radiation involves the measurement of radiation intensity and activity. There are numerous applications in the fields of industry and health in which ionizing radiation is used. Therefore, studies related to the improvement of radiation detectors hold great importance in these fields.

Neutral atoms or molecules acquire positive or negative electrical charge by ionizing radiation. Alpha, beta, and gamma rays; X-rays; and neutron rays are among the most commonly known types of ionizing radiation. As a form of energy, radiation can be stored in a suitable medium, partly or as a whole, and it is capable of producing an effect (Flakus, 2016).

Barnett et al. (1996) described the interaction of particles with matter, the result of such interaction, related calculations, and the Bethe-Bloch formula. Ionization-based mean energy loss is given by the Bethe-Bloch formula (Barnett et al., 1996; Leo, 1992). The basic principle of interaction in matter depends on the type of incident radiation and the particles' energy (Tsoulfanidis, 1995; Leroy and Rancoita, 2009).

Semiconductors and *PN* diodes comprise the basis of all radiation detectors. Semiconductor devices are characterized by basic physical processes and equations including the equilibrium concentration of electron–hole pairs, mobility, bias voltage, and charge density (Sze, 1981; Mishra and Singh, 2008).

The counting efficiency in the radioactivity measurement may

* Corresponding author.
*E-mail addresses:* firdevsbanuozdemir@beykent.edu.tr (F.B. Ozdemir), birkan.selcuk@idu.edu.tr (A.B. Selcuk), suat.ozkorucuklu@istanbul.edu.tr (S. Ozkorucuklu), balpat@sabanciuniv.edu (A.B. Alpat), tozdemir@bartin.edu.tr (T. Ozdemir), nuriozek@sdu.edu.tr (N. Özek).

https://doi.org/10.1016/j.apradiso.2018.01.016
Received 7 February 2017; Received in revised form 21 November 2017; Accepted 12 January 2018
Available online 19 January 2018
0969-8043/ 

**Table 1**
Rn-222 decay products from U-238 chain (Alpat et al., 2007; Lbnl Web page: ⟨http://ie.lbl.gov/toi/radSearch.aspS⟩).

| Radioisotope | Half-life | α | β | γ |
|---|---|---|---|---|
| $^{222}$Rn | 3.823 days | 5490 keV | | 510 keV |
| $^{218}$Po | 3.11 min | 6003 keV | | |
| $^{214}$Pb | 26.8 min | | 7300 keV | |
| $^{214}$Bi | 19.9 min | | 1510 keV | 610 keV |
| $^{214}$Po | 164.3 μs | 7687 keV | | 800 keV |
| $^{21°}$Pb | 21.8 years | | 200 keV | 46 keV |
| $^{21°}$Bi | 5.01 days | | 1160 keV | |
| $^{210}$Po | 138.4 days | 5297 keV | | |
| $^{206}$Pb | Stable | | | |

depend on several factors including composition, geometry, activity, density, placement, radiation type, radiation energy, and other instrument-specific factors. Calculation of estimated efficiency can be explicitly performed as a function of these variables (MARLAP, 2014).

In principle, radiation detectors produce an output signal through interaction within the active volume of the detector. This interaction occurs as ionization and excitation of charged radiation particles such as alpha and beta particles. In the detector, the incident charged particles such as electrons and protons interact with the detector material, thereby producing electron–hole pairs along their trajectories. The count information of charged particles is processed by signal processing electronics upon collection. The detection efficiency of gamma rays and neutrons is generally lower than that of charged particles (Byun, 2016).

Radon and its decay products account for almost 55% of the current radiation dose in the USA (Miller, 2000). Radon (Rn-222) is a radioactive decay product of uranium and thoron series, and monitoring of radon is required in risk areas because of its carcinogenic nature (UNSCEAR, 2008). Radon (Rn-222) is a radioactive decay product of the U-238 chain (Table 1).

Radon, which is one of the naturally occurring radioactive inert gases in the U-238 series, is a product of α radiation of Ra-226 and has a radioactive half-life of 3.84 days. Thoron (Rn-220) and actinon (Rn-219) are the known isotopes of this colorless, tasteless, and odorless gas and have significantly shorter half-lives of 55 and 3.9 s, respectively. Accordingly, radon element is dominated by Rn-222 (UNSCEAR, 1988).

Rn-222 and Ra-226 are among the most common radionucleotides that pose serious health risks for humans. These radioactive elements with high radiation levels threaten human health by inflicting damage in lungs and other organs, upon inhalation through the respiratory tract (Marques et al., 2004). Because of its low affinity, radon does not chemically bond with tissues when inhaled, and its solubility in the tissues is very low. However, radon decay products are retained in dust and other particles, thereby producing inhalable radioactive aerosols. When inhaled, radon gas takes the particle form, which can be retained in lungs. Thus, it is taken into the body through the respiratory tract and emits radiation in every stage of the decay process until it becomes stable. The energy released as a decay product of these particles, thus, increases the risk of cancer with time (Axelson, 1995; Field et al., 2000; UNSCEAR, 2000; Lazar et al., 2003).

Tanaka et al. investigated the number of counts needed to measure radon concentration using the AlphaGUARD (a low-effective volume detector) and compared the values with those of more sensitive radiation detectors (Tanaka et al., 2017). Sharma et al. measured and evaluated mean radon concentration in water samples which ranged between 1.4 ± 0.3 and 13.3 ± 4.1 Bq $1^{-1}$ (Sharma et al., 2017). Testing and calibration results for a gamma-spectrometric complex based on xenon gamma-ray detector were described by Novikov et al. (2017).

Dalla Betta et al. designed and realized a radon sensor using a bipolar junction transistor (BJT), fabricated on a high-resistivity silicon substrate. The functional testing of the proposed system was provided elsewhere (Dalla Betta et al., 2013).

Silicon PIN diode-based electron-gamma coincidence detector system for noble gas monitoring, expected sensitivity, and improvements of the detector system were presented by Khrustaleva et al. (2017).

Geant4 is a toolkit used for the simulation of particle passage through matter. Its functionalities include tracking, geometry, physics models, and number of hits for use in a vast number of experiments and applications including high-energy physics, medical physics, astrophysics, space science, and radiation protection (Agostinelli et al., 2003; Allison et al., 2006).

Radiation is measured following the interaction of particles with matter. The interaction mechanism that depends on the particle's type, energy ($E$) , number of protons ($p$) in the medium of the incident particles, and atom density ($\rho$) is essential for understanding the physical processes. Numerous physical models have been used to initiate and analyze the interaction of particles with matter in a wide energy range (250 eV to 100 TeV). These physical models are electron, positron, photon, charged hadron, and ion interactions; electromagnetic processes; hadron physics involving muon and gamma core interactions; and subatomic decay.

In the simulation study, the efficiencies of thin and thick detectors, that were calculated separately, were named “efficiency,” and the efficiency of both detectors was named the “total efficiency."

HIPRAD detector, introduced in the present study, can separate α, β, and γ particles, and anticoincidence system can prevent the effects of cosmic rays. In this experiment, the Ra-226 isotope was used as the source. Our goal in this study was to measure the Rn-222 activity obtained from the Ra-226 source, whose activity is presented in Table 1. An application of this detector is a prototype of radiation measurement system. The aim of this study was to experimentally detect radon (Rn-222) activity in HIPRAD detector that measures the energy of particles. This study summarizes the energies of alpha, beta, and gamma particles; charge distributions; eta-charge distributions; dose–response values measured in the inner and outer sides of strips; background; and efficiency of radiation detector as shown in the graphical results. Simultaneous alpha and beta measurement capability of the silicon radiation detector was verified with the experimental and simulation results. The experimental spectra of Rn-222 source were theoretically compared with the simulation results on Geant4 and root programs.

## 2. Materials and methods

Several types of detectors are available for radiation detection. These include gas-filled detectors, scintillation detectors, and semiconductor detectors. Silicon radiation detector is a semiconductor double-sided multichannel (strip) radiation measurement detector. Silicon detectors are used in several applications including accelerator systems, dosimeters, nuclear- and high-energy physics experiments, in the field of medical imaging, and in the determination and diagnosis of charged particles. High-precision multisilicon radiation detectors are used to measure the charge, energy, and observation times of alpha, beta, and gamma radiations in solid, liquid, and gas samples. Radiation detectors also measure the dose and activity with high precision. Several studies on the properties of silicon sensors and the performance of detector systems are available in the literature (Leo, 1992; Sze, 1981; Lutz, 1999; .Spieler, 2005).

The multichannel silicon detector (HIPRAD) is shown in Fig. 1. The radiation detector system is equipped with an anticoincidence system, pneumatic system, rechargeable battery-based power supply system, and wireless data transfer system. The anticoincidence system consists of plastic scintillators to eliminate the background radiation induced by cosmic rays (TAEK Turkish Atomic Energy Authority SANAEM Sarayköy Nuclear Research and Training Center, 2012; MAPRad, 2010).

The silicon radiation system consists of a double-sided silicon strip detector. The thin detector in HIPRAD has the dimensions of 7 cm ×

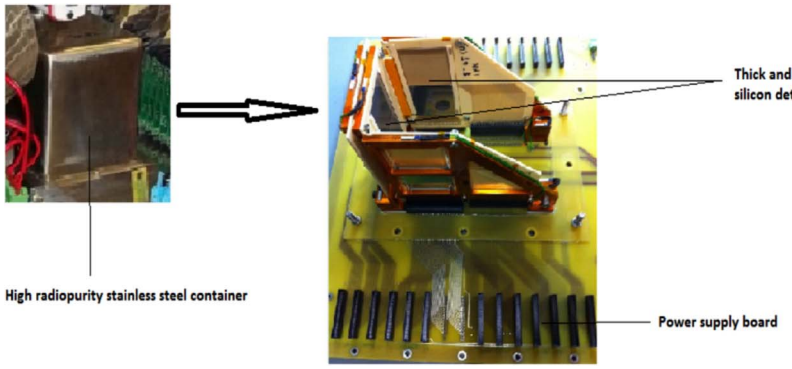


**Fig. 1.** Multisilicon radiation detector (top) and interior design of double-sided microstrip silicon detector with thin (300 μm) and thick (1500 μm; bottom) detectors (MAPRad, 2010).

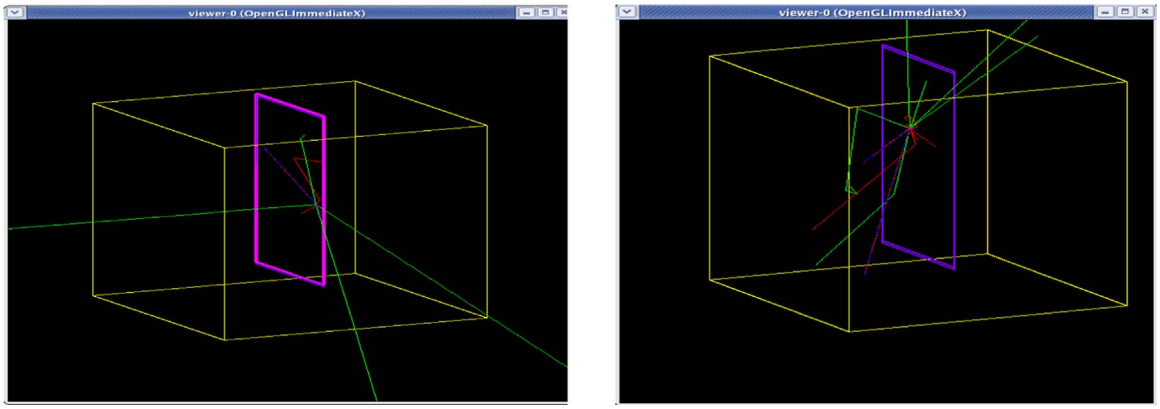


**Fig. 2.** Images of thin and thick silicon detectors simulated using the OpenGLImmediateX (OGLIX) interface in Geant4 program.

4 cm × 300 μm and 196 × 64 channels, and it is supplied with a bias voltage of 100 V. The thick detector has the dimensions of 4 cm × 4 cm × 1.5 mm and 64 × 64 channels, and it is supplied with a bias voltage of 400 V, as shown in Fig. 2 (MAPRad, 2010). The simulated thin and thick detector and the entire system information are provided in the present study.

Silicon detectors generally start to generate noise over 23$^{0}$C. The first measurements with HIPRAD detector were made under standard clean room conditions. In clean room standards, humidity is generally maintained at a constant level between 20% and 40%. In this research, the measurements were performed at 20 $^{0}$C and 30% humidity.

## 3. Computational details

Simulation studies were performed with the Geant4 toolkit, which can simulate the transport of particles through matter by using CLHEP libraries on the Scientific Linux operating system. The particle properties, physical interactions, and the energy deposited in the detector were simulated using the Geant4 program. The state of the particles in the silicon detector was explained by the physics classes in the program.

The thin and thick silicon detectors were simulated using the OpenGLImmediateX (OGLIX) interface in Geant4 program (Fig. 2). The Geant4 simulation work flow generally involves the definition of geometry (including material, volume, location, and units), physical processes (including particles, physics process, and thresholds and cut), event, visualization (the geometry of multisilicon strip detector and trajectories of particles), and acquisition of outputs through user interface (Introduction to Geant4, 2014).

Root is an open-source, C++-dependent, and object-oriented framework, which is used in a wide range of areas, including several experiments in high-energy physics and astrophysics. In the present study, the raw data obtained from the simulation and experimental work was analyzed using this program (Root, 2015; Acas et al., 2008). In this study, the number of particles in the thick and thin detectors and the efficiency of the silicon detector were determined, and these were compared with the results of other studies. The detection efficiency for alpha, beta, and gamma particles was evaluated in terms of the corresponding number of detected particles. The efficiencies for alpha, beta, and gamma particles in the thin detector were 9.02%, 0.036%, and 10.18%, respectively, as listed in Table 2. The efficiencies for alpha, beta, and gamma particles in the thick detector were 9.045%, 0.0346%, and 10.437%, respectively, as listed in Table 2. The total efficiencies for alpha, beta, and gamma particles in the detector were 17.93%, 0.1%, and 50.95%, respectively (Ozdemir et al., 2014, 2012).

In radiation measurement, the fundamental principles of particle interactions in matter depend on the type and energy of the incident radiation (Tsoulfanidis, 1995; Leroy and Rancoita, 2009). Fig. 3 shows the kinetic energies of alpha, beta, and gamma particles and their distribution in the detector simulation. Particles with energies higher than 5 MeV are defined as alpha particles, particle entries with energies between 0.046 and 1.76 MeV are defined as gamma particles, and those between 0.02 and 3.26 MeV are defined as beta particles.

## 4. Experimental details

Experimental studies were conducted in air medium. The detector was tested using 13.6-kBq Rn-222 source. The measurement period was 45 min for background and 15 min for Rn-222 source. The alpha-particle and beta-particle spectra, eta-charge distributions, and charge distributions of Rn-222 source in the N and P sides of multisilicon strip detector were obtained. The half-life and the activity of Rn-222 are given in Table 3.

Radiation detectors can measure the energy value of a released particle, thus enabling particle identification during the decaying process. A specific decay process can always be determined with a given isotope using the characteristics of the generated signal. Furthermore, in the electronic section, the data acquisition (DAQ) system is composed of numerous electronic boards, each having specific tasks. These

**Table 2**
Number of alpha, beta, and gamma particles formed in thin and thick detectors and efficiency percentage, in Geant4 simulation.

| Thin detector | | Thick detector | |
|---|---|---|---|
| **Event numbers** | 10000 | **Event numbers** | 10000 |
| Number of alpha particles in "world volume"[a] | 40000 | Number of alpha particles in "world" volume | 40000 |
| Number of beta particles in world volume | 19901793 | Number of beta particles in "world" volume | 19902914 |
| Number of gamma particles in world volume | 28469 | Number of gamma particles in "world" volume | 28446 |
| Number of alpha particles in thin silicon detector | 3607 | Number of alpha particles in thick silicon detector | 3618 |
| Number of beta particles in thin silicon detector | 7103 | Number of beta particles in thick silicon detector | 6884 |
| Number of gamma particles in thin silicon detector | 2898 | Number of gamma particles in thick silicon detector | 2969 |
| Number of alpha particles from Po-214 in thin silicon detector | 907 | Number of alpha particles from Po-214 in thick silicon detector | 883 |
| Number of beta particles from Bi-214 in thin silicon detector | 1279 | Number of beta particles from Bi-214 in thick silicon detector | 1339 |
| **Efficiency** | **%** | **Efficiency** | **%** |
| Alpha | 9.02 | Alpha | 9.045 |
| Beta | 0.036 | Beta | 0.0346 |
| Gamma | 10.18 | Gamma | 10.437 |

[a] The largest volume in the detector geometry is called the world volume in Geant4.

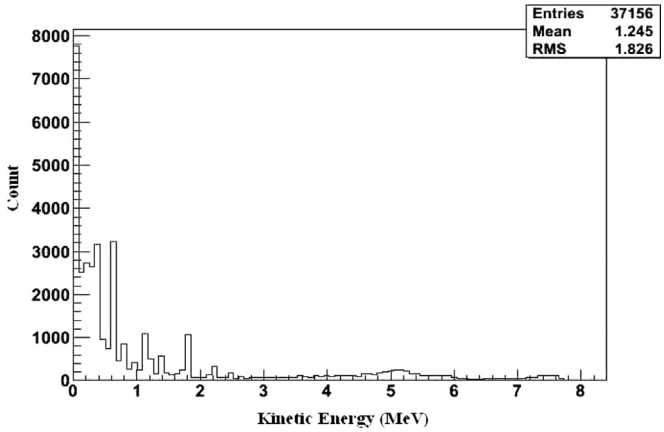


**Fig. 3.** Kinetic energies of alpha, beta, and gamma particles, decaying from $^{222}$Rn.

**Table 3**
Half-life and activity of Radon-222.

| Radioisotope | Half-life | Reference date | Activity | Resulting particle |
|---|---|---|---|---|
| Rn-222 | 3.82 days | 01.06.2012 | 19.6 kBq | α |

boards include the power supply boards, which supply electrical power to various DAQ parts, master DAQ board for system coordination, slave DAQ (secondary acquisition boards) for each side of thin and thick sensors, and front-end boards, which are independent from the PCB (TAEK, 2014).

Multisilicon radiation detector features different operating conditions for data acquisition. These are high vacuum, trap mode, and sniff mode. High vacuum mode involves radioactive source measurements of solid samples placed at the center of the silicon detector, the measurements in air media, and the measurements made to determine the background radiation that are performed under approximately $10^{-6}$ mbar. Trap mode involves the measurements made less than 1 atm pressure for calibration and concentration measurements at the center of the silicon detector. Sniff mode is used for continuous sampling activity, while the air flows through the center of the detector. Background radiation measurements are made under high vacuum for both trap mode and sniff mode, and background measurement values are subtracted from radon measurement values. Throughout this sampling process, all analog values of microstrip silicon detector were read and recorded for all particle events along with the time stamp, slow control data, and environmental parameters for each trigger (Alpat et al., 2007).

The efficiency of the detector depends on the mean critical angle and the response function $V(R_D)$ (Nadir et al., 2014). In the simulation, the absolute efficiency of alpha decay measurement from Rn-222 was found to be 17%.

In this study, the specimens were confined in a container, and a balloon was attached to the outlet valve of the container to equalize the internal and external pressure, as shown in Fig. 4. Experimental measurements were performed on the high-sensitivity silicon radiation detector (HIPRAD). The simulation data of radiation detector were used to obtain the radioactive decay, energy generation, energy values, and efficiency values. Radon measurements were made experimentally using the Rn-222 source. Charge distributions, counts based on the number of channels, and eta distributions on K and S edges are shown in Figs. 5–7, respectively.

The charge distribution in P (inner) and N (outer) sides was separately observed. An amplifier was connected to the computer using an analog to digital converter (ADC). The ADC channel count, counts in strips, and charge distribution in the N (exterior) side were lower than those in the P side. The count graphs were given for the K and S edges depending on the ADC channel, as shown in Figs. 5 and 6, respectively. Background measurement was made before placing the source. Corrected charge distributions are obtained by subtracting the background data from the real data, as shown in Figs. 5 and 6.

The ADC channel range of radiation detection is between 0 and 4096. The electronic system of the device is calibrated at 10 MeV. The 4096 channels range between 0 and 10 MeV. Therefore, the ADC

**Fig. 4.** The container.

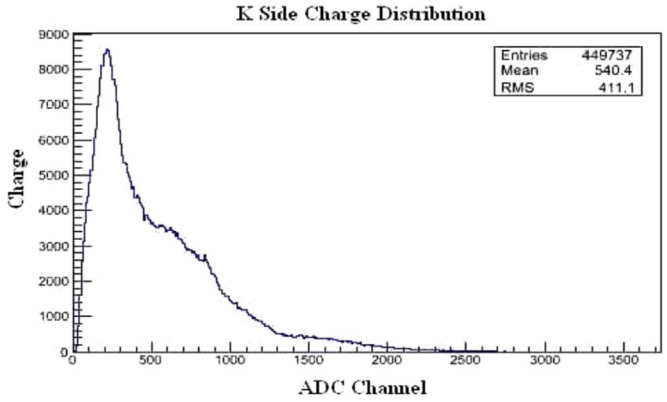


**Fig. 5.** Corrected charge distribution in the K (inner) side of the detector by Rn-222 source in air.

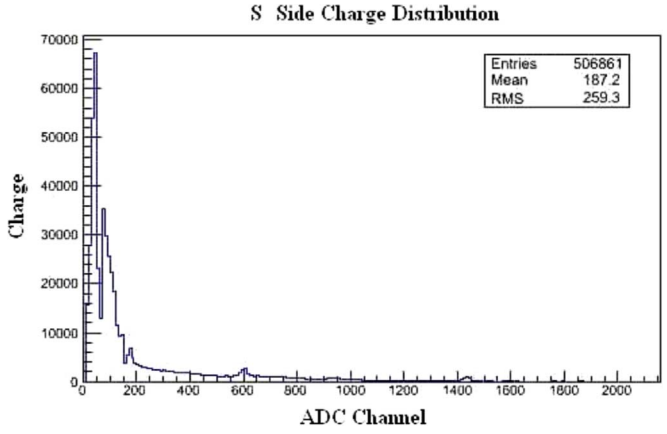


**Fig. 6.** Corrected charge distribution in the S side (outer) of the detector by Rn-222 source in air.

channel can be called as the energy gap.

The smallest difference in energy between α, β, and γ particles coming out of the decay products of Rn-222 was 100 keV. The energy value corresponding to each channel is 10 MeV / 4096 = 0.0024 MeV = 2.4 keV. Thus, 100 keV / 2.4 keV = 42 channels would be sufficient for more than 10 intervals to distinguish the coming particle. The difference between the energies of the daughter nucleus products of Rn-222 in the detector corresponded to a minimum of 100 keV / 2.4 keV = 42 channels, which would be sufficient to distinguish the particle.

Full width at half maximum (FWHM) (Knoll, 2000) represents the width when the peak count of HIPRAD silicon detector is reduced by half and it is calculated as follows: $2\sigma\sqrt{2\ln 2}$. Here, $\sigma$ denotes the standard deviation of the peak.

As shown in Fig. 5, the average value of the peak between channels 0 and 1048 and the sigma value are 702 and 446, respectively. Here, the FWHM was calculated as 1048 keV using the equation $\mathrm{FWHM} = 2\sigma\sqrt{2\ln 2} = 2.35\,\sigma$.

R value was found as 1.49 from the equation $R = \frac{FWHM}{H_0}$

The silicon strips in the detector are two sided. "K" refers to the inner side and “S" refers to the outer side of the silicon detector. The charge distributions in K (inner) and S (outer) sides of the silicon detector are separately given in Figs. 5 and 6, respectively. The ADC channel count, strip count, and charge distributions observed on the S side of the detector were lower than those observed on the K side. This difference in S side can be ascribed to the lower mobility of the holes.

Fig. 7 shows the eta-charge distributions of Rn-222. Because the alpha particles lose energy in the thin silicon in air environment, the eta-charge distribution graph seems to be free from ambiguity. The alpha particles composed of different decays in Rn-222 decay were clustered in different eta values. The eta value determines where charges are grouped in the right and left charge distributions of strips, and it ranges between 0 and 1 in the *x*-coordinate. Eta value was calculated using the following equation ($\mathrm{Eta} = Q_{left}/(Q_{right} + Q_{left})$ (Alpat et al., 2007).

Each count per minute corresponds to activity value on the inner and outer side of the silicon strips in dose-response graphs. High-precision radiation detector has a reliability of 95% as given shown in Fig. 8. The numbers outside the linear line represent incorrect data. These errors are due to voltage variations and changes in threshold value and detector noise.

## 5. Conclusion

Silicon-based radiation detector for Rn-222 source was simulated, and alpha, beta, and gamma particle detection efficiencies of the detector were calculated in this study. The experimental study was conducted using the standard source. In the obtained data, the values of the first 160 channels correspond to the S edge and those of the next 288 channels correspond to the K edge. The difference between the occupancy rates of the channels on the K and S edges is attributed to the location of the source inside the detector and close to the K edge, its particle's relatively different range, and its inability to reach the S edge of the detector. The silicon strips in the detector are in the *PN* structure. The S edge is a “P-type” carrier, whereas the K edge is an “N-type” carrier. The K edge is likely to have denser charge distributions because of its free-electron-rich “N-type” semiconductor characteristic. The charge distribution is less dense in the vacancy-rich “type P” carrier S edge. The energy of alpha particles dissipates at short distance, and these particles are characterized with energy loss (Bethe-Bloch) while passing through a material. Measurement of counts will depend on various characteristics such as the geometry, diameter of the source, absorption in air, detector window and the distribution of the particles.

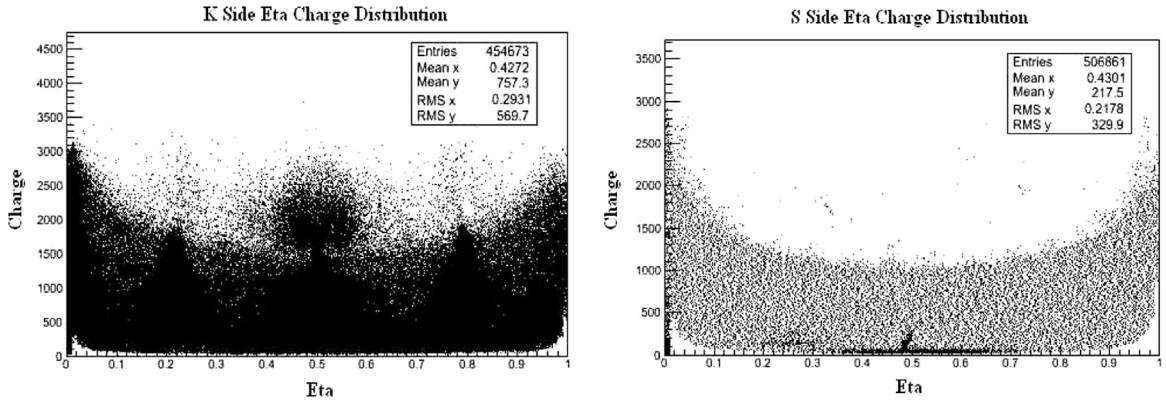


**Fig. 7.** Eta-charge distributions.

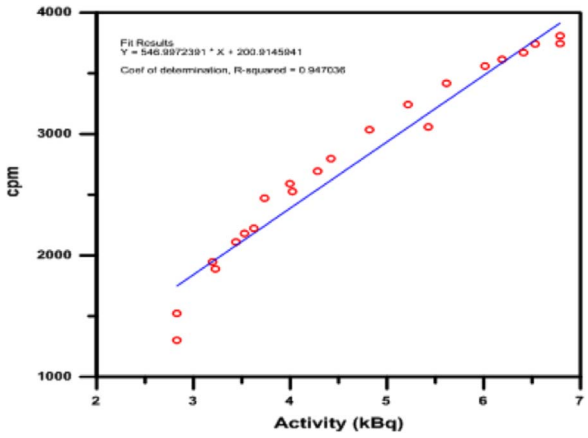


**Fig. 8.** Rn-222 Dose–Response graphs obtained for the inner and outer sides of strips.

In air, the corrected charge distribution in the K (inner) and S (exterior) sides of the detector by Rn-222 source was obtained by subtracting the background data from the real data and is shown in Figs. 5 and 6, respectively. The dose–response graphs of $^{222}$Rn for the K (interior) and S (exterior) sides of the silicon radiation detector indicate that the detector has 95% reliability (Fig. 8).

## Acknowledgements

The authors gratefully acknowledge the technical support of TAEK (Turkish Atomic Energy Authority-Ankara) and INFN–The National Institute of Nuclear Physics-Perugia.

## References

Acas, R.K., Tripathi, A., ROOT, 2008. A Data Analysis and Data Mining Tool from CERN, Casualty ActuarialSociety *E-Forum*, Winter.
Agostinelli, S., et al., 2003. Geant4-a simulation toolkit. Nuclear Instrum. Methods Phys. Res. Section A: Accelerators, Spectrom. Detect. Assoc. Equip. 506, 250–303.
Allison, J., et al., 2006. Geant4 developments and applications. IEEE Trans. Nucl. Sci. 53–1, 270–278.
Alpat, B., Aisa, D., Bizarri, M., Blasko, S., et al., 2007. Multipurpose high sensitivity radiation detector: Terradex. Nucl. Instrum. Methods Phys. Res. A 574, 479–492.
Axelson, O., 1995. Cancer risks from exposure to radon in homes. Environ. Health Persp. 103 (2), 37–43.
Barnett, R.M., et al., 1996. Review of particle properties. Phys. Rev. D54.
Byun, H.S., 2016. Radioisotopes and Radiation Methodology Lecture Notes, Med Phys 4R06/6R03.
Dalla Betta, G.F., Tyzhnevyi, V., Bosi, A., et al., 2013. Nuclear Instrum. Methods Phys. Res. A 718, 302–304.
Field, R.W., Steck, D.J., Smith, B.J., Brus, C.P., Neuberger, J.S., Fisher, E.F., Plats, C.E., Robinson, R.A., Woolson, R.F., Lynch, C.F., 2000. Residential gas exposure and lung cancer: the Iowa radon lung cancer study. Am. J. Epidemiol. 151 (11), 101–102.
Flakus, F.N., 2016. Detecting and measuring ionizing radiation - a short history, radiation detection. IAEA Bull. 23 (4).
Introduction to Geant4, available at ⟨http://geant4.web.cern.ch/geant4/UserDocumentation/UsersGuides/IntroductionToGeant4/html/index.html⟩ (Accessed on 24 Aug 2014).
Khrustaleva, K., Popov, Yu, Popov, V., Yu, S., 2017. Appl. Radiat. Isot. 126, 237–239.
Knoll, G.F., 2000. Radiation Protection and Measurement. John Wiley&Sons, Inc, Newyork.
Lazar, I., Toth, E., Marx, G., Cziegler, I., Kotdes, G.J., 2003. Effects of residential radon on cancer incidence. J. Radioanal. Chem. 258 (3), 519–524.
Lbnl Web page: ⟨http://ie.lbl.gov/toi/radSearch.aspS⟩.
Leo, W.R., 1992. Techniques for Nuclear and Particle Physics Experiments: A How to Approach. Springer-Verlag, Berlin Heidelberg, Germany.
Leroy, C., Rancoita, P.G., 2009. Principles of Radiation Interaction in Matter and Detection. World Scientific publishing Co. Pte. Ltd.
Lutz, G., 1999. Semiconductor Radiation Detectors. Springer-Verlag, Berlin Heidelberg.
MAPRad, 2010. Available at ⟨http://www.maprad.com/en/index.php?Content=Products.html⟩ (Accessed on 05 July 2016).
MARLAP, 2014. available at ⟨http://www.epa.gov/radiation/marlap/manual.html⟩ (Accessed 11 May 2014).
Marques, A.L., Santos, W., Geraldo, L.P., 2004. Direct measurements of radon activity in water from various natural sources using nuclear track detectors. Appl. Radiat. Isot. 60 (6), 801–804.
Miller, G.T., 2000. Living in the Environment: Principles, Connections, and Solutions, 11th ed. Brooks/Cole, USA.
Mishra, U.M., Singh, J., 2008. Semiconductor Device Physics and Design. Springer, The Netherland.
Nadir, A.F., Subber, A.R.H., Al-Hashmi, N.H.N., 2014. Arch. Phys. Res. 5 (5), 23–30.
Novikov, A., Ulin, S., Dmitrenko, V., Chernysheva, I., Grachev, V., Vlasik, K., Uteshev, Z., Shustov, A., Petrenko, D., Bychkova, O., 2017. Radon concentration monitoring using xenon gamma-ray spectrometer. IOP Conf. Series: J. Phys. Conf. Ser. 798.
Ozdemir, F.B., Ozdemir, T., Ozkorucuklu, S., 2012. Bir Silikon Mikro-Şerit Dedektörün Yapısı ve Benzetimle Performans Çalışması. In: Abs. Proceedings 29th International Physics Congress, Turkish Physics Institution, 29/280.
Ozdemir, F.B., Alpat, B., Selçuk, A.B., Ozkorucuklu, S., Ozdemir, T., 2014. The experimental measurement methods and the simulation study of high-precision radiation detector. In: Abs. Proceedings 31st International Physics Congress, Turkish Physics Institution, 31, 96.
Root, 2015. Available at ⟨http://root.cern.ch/root/ExApplications.html⟩ (Accessed on 23 August 2015).
Sharma, S., Duggal, V., Srivastava, A.K., Mehra, R., 2017. Assessment of Radiation Dose from Exposure to Radon in Drinking Water from Western Haryana, India. Int. J. Environ. Res. 11, 141–147.
Spieler, H., 2005. Semiconductor Detector Systems. Oxford University Press Inc, New York.
Sze, S.M., 1981. Physics of Semiconductor Devices, 2nd ed. Wiley, New York.
TAEK, 2014. Project number: A3.H3.P1.02.
TAEK (Turkish Atomic Energy Authority) SANAEM (Sarayköy Nuclear Research and Training Center), 2012. High Sensitivity Radiation Detector, available at ⟨http://www.taek.gov.tr/sanaem/30-arastirma-ve-gelistirme-bolumu/965-yuksekhassasiyetli-radyasyon-dedektorunun-Çok Silikonlu Radyasyon Dedektörü-testleri-sa-naemde-basladi.html⟩ (Accessed on 02 January 2012).
Tanaka, A., Minami, N., Yasuoka, Y., Limoto, T., Omori, Y., Nagahama, H., Muto, J., Mukai, T., 2017. Accurate Measurement of İndoor radon concentration using a low-effective volume radon monitor. Radiat. Prot. Dosim. 1–7.
Tsoulfanidis, N., 1995. Measurement and Detection of Radiation. Taylor & Francis, USA.
UNSCEAR, 1988. Sources, Effects and Risks of Ionizing Radiation. UN, New York.
UNSCEAR, 2000. Exposure Due to Natural Radiation Sources. United Nations, New York.
UNSCEAR, Sources and Effects of Ionizing Radiation. Report to General Assembly with Scientifc Annexes, vol. 1., 2008.